J Mater Sci (2013) 48:4626–4636
DOI 10.1007/s10853-013-7254-4

NANOSTRUCTURED MATERIALS

Adiabatic heating and the saturation of grain refinement during SPD of metals and alloys: experimental assessment and computer modeling

A. P. Zhilyaev · S. Swaminathan · A. I. Pshenichnyuk · T. G. Langdon · T. R. McNelley

Received: 29 November 2012 / Accepted: 20 February 2013 / Published online: 5 March 2013

Abstract Severe plastic deformation methods include equal-channel angular pressing/extrusion, high-pressure torsion, and plane strain machining. These methods are extremely effective in producing bulk microstructure refinement and are generally initiated at a low homologous temperature. The resulting deformation-induced microstructures exhibit progressively refined cellular dislocation structures during the initial stages of straining that give way to refined, equiaxed grain structures at larger strains. Often, grain refinement appears to saturate but frequently coarsening is observed at the largest strains after a minimum in grain size is attained during SPD. Here, we summarize results on grain refinement by these processing methods and provide an analysis that incorporates adiabatic heating to explain the progressive refinement to intermediate strains and that may be followed either by an apparent saturation in grain refinement or by grain coarsening at the largest strains. This analysis is consistent with continuous dynamic recrystallization in the absence of the formation and long-range migration of high-angle boundaries.

A. P. Zhilyaev · T. G. Langdon
Materials Research Group, Faculty of Engineering and the Environment, University of Southampton, Southampton SO17 1BJ, UK

A. P. Zhilyaev · A. I. Pshenichnyuk
Institute for Metals Superplasticity Problems, Russian Academy of Science, 39 Khalturnia Street, Ufa 450001, Russia

S. Swaminathan
John F Welch Technology Center, GE Global Research, Bangalore 560066, India

T. G. Langdon
Departments of Aerospace & Mechanical Engineering and Materials Science, University of Southern California, Los Angeles, CA 90089-1453, USA

T. R. McNelley (✉)
Department of Mechanical and Aerospace Engineering, Naval Postgraduate School, Monterey, CA 93943-5146, USA
e-mail: tmcnelley@nps.edu

Introduction

The potential to achieve extraordinary refinement of grain structures in bulk materials by severe plastic deformation (SPD) methods was first recognized by Valiev [1] in work examining the suitability of the equal-channel angular pressing (ECAP) [2] process for refinement of grain size. Equivalent strains of ten or more have been attained by repetitive ECAP of bulk samples at ambient temperature. Both pure metals and alloys [3] have been processed by ECAP methods. The production of submicron and even nano-scale grains with high-angle grain boundaries by repetitive ECAP has been demonstrated in numerous reports [4–7]. In high-pressure torsion (HPT),a material is subjected to large hydrostatic pressure while simultaneously being strained in torsion [8]; the process akin to that suggested by Bridgman [9, 10]. Indeed, equivalent strains greatly exceeding those attainable in repetitive ECAP have been achieved by HPT although strain variations from the center to the periphery of sample discs complicate their assessment and the material's constitutive behavior. Another bulk deformation method is plane strain machining (PSM) wherein large strains are introduced in the chips produced by the PSM process [11], resulting in highly refined grain structures. While there are other interesting SPD methods, such as accumulative roll bonding (ARB), twist extrusion (TE) and cold or warm torsion

straining, the scope of this work will be confined to ECAP, HPT, and PSM.

Usually, SPD processes are initiated at ambient temperature, which corresponds to a low homologous temperature, i.e., $T_{SPD} \leq 0.3T_M$, for metallic materials such as Al, Cu, Ni, or Fe. The introduction of cellular dislocation structures that evolve into highly refined grain structures will lead to a progressive increase in flow stress and a corresponding increase in the rate of energy dissipation for SPD processing at a constant nominal strain rate and low homologous temperature. Approximately isothermal conditions may prevail at low deformation rates in an apparatus that has a good heat sink capability and the initial temperature would then represent a lower bound for the deformation temperature. However, if deformation takes place under adiabatic conditions, such as due to high deformation rates, the sample temperature will increase continually during deformation. Nevertheless, predictive models [12] of microstructure evolution during SPD have assumed isothermal conditions, while application of finite element methods to estimation of the temperature rise has suggested that it is limited, at least in some cases [13].

Indeed, few direct measurements of temperature changes during SPD processing have been reported. Yamaguchi et al. [14] used thermocouples embedded in billets and measured temperature increases of 25–30 °C during an ECAP pass on initially annealed pure aluminum. Zhilyaev et al. [15] inferred a temperature rise of ~140 °C during HPT of an as-cast Na-modified Al–7 wt% Si alloy based on changes in precipitate distributions. Finally, Todaka et al. [16], used a thermocouple embedded in the upper anvil of an HPT apparatus to measure temperature changes at a location ~1 mm above the upper surface of high-purity aluminum samples. The samples were 0.85 mm in thickness and 10 mm in diameter. The temperature increased from 20 to ~45 °C during ten revolutions at 5 rpm, while corresponding measurements for a sample deformed at 0.2 rpm indicated a temperature increase from about 18–20 °C so that there was a much smaller increase at the lower deformation rate. When another sample was deformed at 5 rpm after being cooled to an initial temperature of about −75 °C, the temperature increased more rapidly than for deformation at ambient temperature and rose to −40 °C after only three revolutions, representing a temperature change of approximately 35 °C. In contrast, during chip formation in PSM shear plane temperatures as high as T_M could be realized with appropriate machining conditions [17].

Clearly, SPD processing may involve significant temperature increases, although the extent of the temperature change will depend on the material as well as the experimental conditions. Microstructure evolution during SPD at low homologous temperatures will probably be influenced by both the initial deformation temperature and any adiabatic effects. Thus, questions such as whether cell or grain size saturates during straining, and what are the related recovery and recrystallization mechanisms, remain to be fully answered. Furthermore, assessments of the deformation mechanisms at extreme strains and the role of alloy constitution will also depend on the thermo-mechanical history during SPD processing.

In the following sections, SPD processing by ECAP, HPT, and PSM will be reviewed and selected examples of microstructure evolution summarized. Based on the microstructures observed, an analysis of adiabatic effects on the accumulation of plastic deformation energy in the microstructure and the evolution of microstructure parameters has been developed to elucidate the microstructure transformation observed during SPD.

Experimental: ECAP, HPT, and PSM

The details of an ECAP apparatus design and processing have been given in numerous reports (e.g. [3]). Briefly, an ECAP die comprises two channels of equal cross-section that intersect at an angle, as shown in the schematic of Fig. 1a. Dies generally include a relief angle, denoted by ψ in Fig. 1a, at the outer corner of the die channel intersection. A billet pressed through such a die must undergo shear deformation as it passes through the plane of the die channel intersection. Because the die entrance and exit channels have the same cross-section, billets can be pressed repetitively as a means to achieve large cumulative strains. Billet rotation between successive ECAP passes controls the strain path during SPD by ECAP. In the absence of billet rotation (route A) or with alternating rotations of the same magnitude (route B_A) the processing path involves monotonically increasing strain, while rotations of 90° between successive passes (route B_C) or 180° (route C) lead to redundant straining every four or two passes, respectively. The cumulative strain, γ_{cum}, during repetitive ECAP may be calculated in terms of the number of passes, N_P, and the shear strain per pass using Eq. 1 [18]:

$$\gamma_{cum} = 2N_P \cot\left(\frac{\varphi}{2} + \frac{\psi}{2}\right) + \operatorname{cosec}\left(\frac{\varphi}{2} + \frac{\psi}{2}\right), \quad (1)$$

where φ is the die channel angle. For a die having $\varphi = 90°$ and $\psi = 0°$, $\gamma = 2N_P$. In the event that large, uniform shear strains are encountered in deformation processing (e.g., as during an ECAP pass) the Hencky relationship [19, 20] between shear and equivalent strains (ε_{eq}) should be used to estimate the latter quantity:

$$\varepsilon_{eq} = \frac{2}{\sqrt{3}} \ln\left(\sqrt{1 + \frac{\gamma^2}{4}} + \frac{\gamma}{2}\right) \quad (2)$$

and the cumulative equivalent strain during repetitive ECAP is then $\varepsilon_{eq.} = 1.02N_P$.

The HPT process has also been described in detail elsewhere [8]. A disc-shaped sample, as illustrated in the schematic of Fig. 1b, is placed under axial compression normal to the plane of the disc and then subjected to torsion about the disc axis. Loading of the sample disc may be accomplished on flat platens (unconstrained HPT) or the sample may be placed in a recess in one or both platens (constrained HPT). For a thin disc (i.e., $2r/h \geq 10$, where r is the disc radius, and h is the disc thickness) friction between the sample surface and the platens under the axial load leads to hydrostatic constraint and torsional deformation under a superimposed hydrostatic pressure. An increment in the shear strain, $d\gamma$, may be estimated from the distortion of the disc in torsion as:

$$d\gamma = \frac{dl}{h} = \frac{r d\theta}{h}, \tag{3}$$

where θ is the angle of twist about the disc axis. In turn, for small strains the shear strain as a function of location in the disc is determined by Eq. 4 as:

$$\gamma = \frac{\theta r}{h} = \frac{2\pi N_T r}{h}, \tag{4}$$

where N_T is the number of turns about the disc axis. In an investigation of HPT of pure Ni under a hydrostatic pressures of 1 GPa or greater, five or more revolutions were attained [16] so that Eq. 4 predicts shear strains of zero at the center of the disc and >100 at the disc periphery. Such an estimate of strains and the strain gradient during HPT neglects strain hardening and load redistribution during deformation and, accordingly, Eq. 4 cannot be applied in a meaningful manner. Nevertheless HPT may involve extraordinarily large strains.

Although it has not been used as extensively in SPD investigations as other methods, PSM is a bulk deformation process that enables very large strains to be introduced in a single deformation stage [21–23]. A schematic of PSM is shown in Fig. 1c. As the cutting tool advances at a speed of v_0 and at a pre-fixed depth of cut a_0, a chip is produced by intense, localized shear on a plane inclined at an angle φ to the direction of tool advance. The face of the tool is termed the rake face and the rake face normal (RFN) is shown in Fig. 1c. Deformation will be plane strain in nature when the chip flow direction (CFD), the RFN, and the direction of v_0 are co-planar. Then, a volume element ABCD will be sheared to A'B'C'D' in the chip and the corresponding shear strain is given by [23]:

$$\gamma = \frac{\cos(\alpha)}{\sin(\phi)\cos(\alpha - \varphi)}, \text{ where}$$

$$\tan(\varphi) = \frac{r\cos(\alpha)}{1 - r\sin(\alpha)} \text{ and } r = \frac{a_0}{a_C}. \tag{5}$$

The angle α is termed the rake face angle, φ is the angle of inclination of the shear plane, and r is the chip thickness ratio. The values of φ and r must be determined by measurement prior to evaluating the shear strain γ after a PSM experiment. From Eq. 5, the shear strain is $\gamma = 2$ for a rake angle $\alpha = 0°$ and chip thickness ratio $r = 1.0$, and this is equivalent to ECAP processing through a 90° die. Even greater shear strains in a single cutting operation may be attained for negative rake angles.

Data on SPD processing of Al, Cu, and Ni materials will be analyzed here to assess the dependence of grain size on strain. Procedures for the various SPD processing techniques have been given in previous report [24]. The resulting microstructures have been evaluated by orientation imaging microscopy (OIM) and transmission electron microscopy (TEM) methods. Procedures for acquisition, analysis, and representation of the OIM data have also been given in previous reports [25–27]. Details of sample preparation, image acquisition, and analysis of TEM data have been provided elsewhere [28, 29].

Results

High-resolution inverse pole figure (IPF) grain maps are shown in Fig. 2 for high-purity Al processed by one ECAP pass (Fig. 2a) and after either four or 12 repetitive ECAP passes by route B_C (Fig. 2b, c, respectively). The grain size

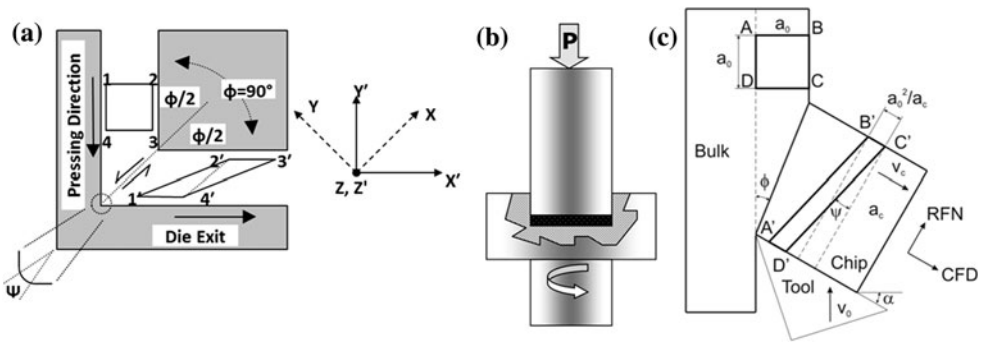

Fig. 1 Schematics of **a** equal-channel angular pressing, **b** high-pressure torsion and **c** plane strain machining

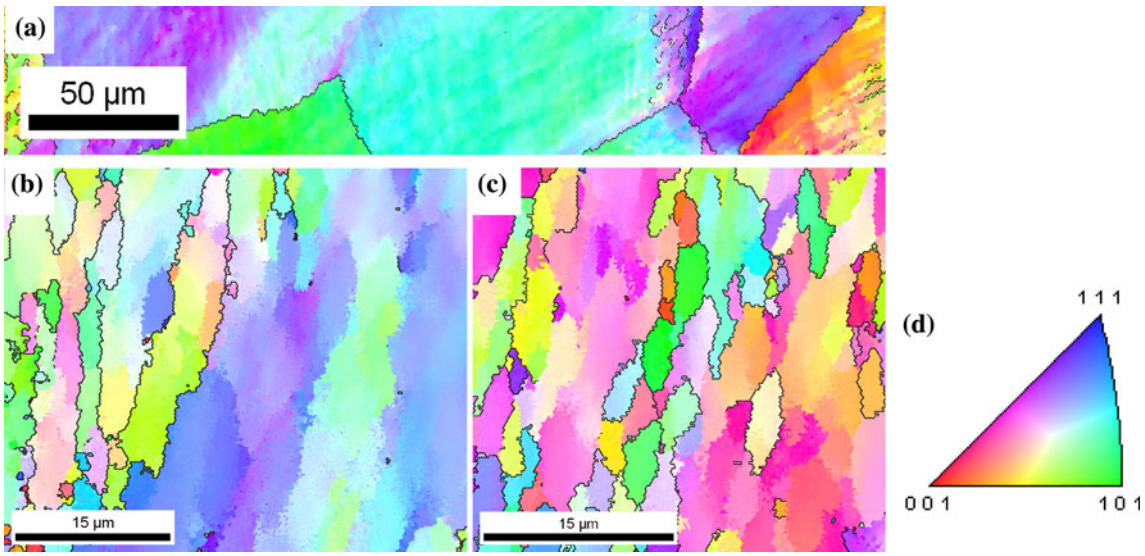

Fig. 2 Inverse pole figure maps of ECAP high-purity aluminum: **a** single pass (grain size is about 50 μm), **b** route B_C 4 passes (grain size ~4.0 μm), **c** route B_C 12 passes (grain size ~3.8 μm), **d** standard stereographic triangle

in the annealed billet was ~1 mm prior to the initial pass [24] and the development of a refined, cellular substructure within very coarse grains is evident in Fig. 2a. The color variation in this IPF map suggests that adjacent cells have small lattice misorientations but that there are also long-range lattice rotations within the prior grains as well. After four ECAP passes by route B_C refined grains have developed, as indicated by the black lines in the IPF map in Fig. 2b, and an even finer substructure is present within these grains. After 12 repetitive ECAP passes by route B_C, the population of high-angle boundaries appears somewhat greater than after four passes and the color variation also suggests greater spread in the distribution of lattice orientations, as seen in Fig. 2c. Mean grain size after four and 12 passes are 4.0 and 3.8 μm, correspondingly, suggestive of saturation of grain refinement after four ECAP passes (an equivalent strain of ≈4.0), at least within the standard deviation of the grain size measurements. Temperature measurements were not included but experimental conditions were similar to those reported by Yamaguchi et al. [12].

Grain refinement during HPT straining of commercial purity Al is summarized in Fig. 3, which shows IPF grain maps acquired on the periphery of sample discs. A refined structure is evident at $N_T = 1$ (Fig. 3a) with grains ~1 μm in size. The uniform color within the grains indicates that the lattice orientation does not vary in the grain interiors and thus the absence of substructure. The grains are ~0.9 μm in size upon straining to $N_T = 2$. No substructure is evident in most of the grains in the IPF map in Fig. 3b (note the difference in magnification). The microstructure remains essentially unchanged during further HPT straining through four as well as eight turns in Fig. 3c, d, suggesting a saturation of grain size at ~0.9–1.0 μm. Again, temperature measurements were not made in the course of this HPT study.

A similar study has employed high-resolution OIM techniques to study refinement of grain size in high-purity Ni after straining by HPT through progressively greater numbers of turns [30]. After the smallest strain, $N_T = 0.1$, the microstructure was dominated by low-angle boundaries in an equiaxed, cellular, or subgrain structure. A finer subgrain structure and increased proportion of high-angle boundaries became apparent in material strained to $N_T = 0.25$. An even finer structure and greater proportion of high-angle boundaries became apparent at $N_T = 0.5$. Indeed, at this strain the boundaries were predominantly high-angle in nature and the grains were reduced to ~200 nm in size. The proportion of high-angle boundaries and the grain size appear to remain constant as N_T increases further to one and even five rotations. Thus, as in the foregoing investigation of grain refinement in commercial purity Al, refinement of grain size in high-purity Ni appears to saturate with straining at a temperature that is nominally ambient although temperature changes during deformation were not documented. Nevertheless, in the Ni study the hardness increased gradually from 1 to 5 turns, while electrical resistivity decreased over this same interval of strain. The latter properties reflect the evolution of the defect structure during straining although such defects may include vacancies and individual dislocations as well as interfaces.

Pure Al and pure Cu were processed by PSM and microstructures as functions of shear strain are illustrated in Figs. 4 and 5, respectively. In PSM, the rake angle, α, and depth of cut, r_0, are set initially. The chip thickness

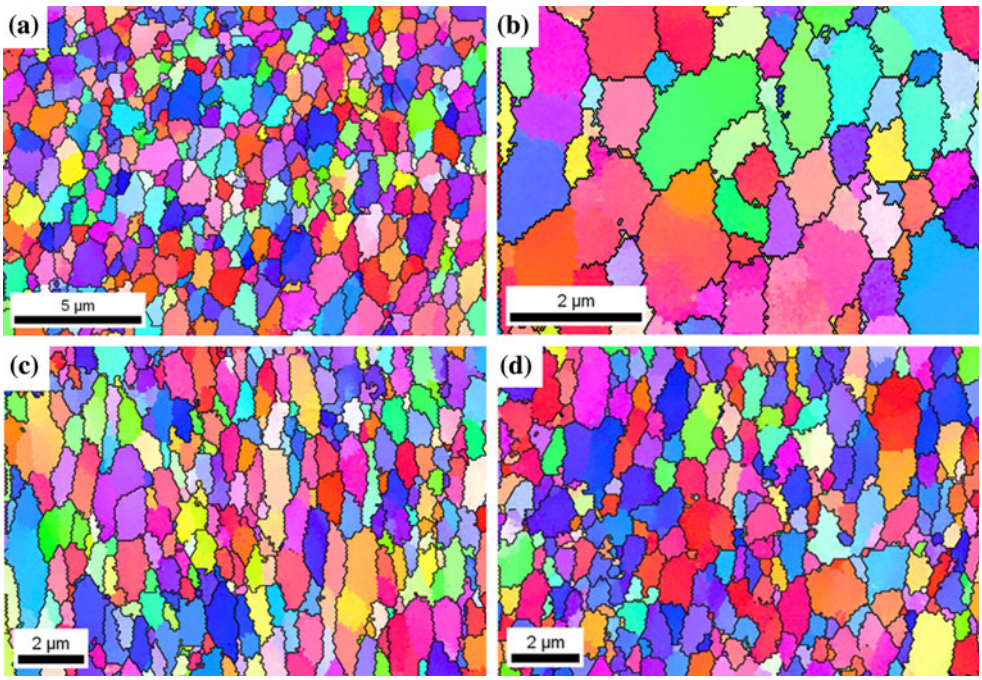

Fig. 3 Inverse pole figure maps of HPT Al ($P = 6$ GPa, room temperature): **a** $N = 1$, edge ($d \sim 1$ μm), **b** $N = 2$ edge ($d \sim 0.9$ μm), **c** $N = 4$, edge ($d \sim 0.95$ μm), and **d** $N = 8$ mid-radius ($d \sim 0.93$ μm)

ratio, r, is measured after completion of the cutting process, and the corresponding shear strain value is then determined by applying Eq. 5. The corresponding equivalent strains may then be calculated by applying Eq. 2. The cutting process was conducted at a speed $v_0 = 8.3$ mm/s for the Al and shear strains ranging from 3.2 to 17.1 (corresponding to equivalent strains ranging from 1.4 to 3.3) were attained. A speed $v_0 = 18.3$ mm/s was employed with the Cu and shear strains from 2.9 to 13.6 (equivalent strains ranging from 1.3 to 3.0) were achieved. Under these machining conditions, temperature changes of up to 50 °C are expected in Al and up to 100 °C in the case of Cu.

During PSM of the pure Al, refined, elongated subgrains approximately 390 nm in size are evident after a shear strain of 3.2 ($\varepsilon_{eq.} = 1.44$) and the subgrains are only slightly finer upon attaining a shear strain of 6.9 ($\varepsilon_{eq.} = 2.25$). An equiaxed structure is evident after shearing to a strain of 10.9 ($\varepsilon_{eq.} = 2.76$) and the grain size of ~ 1.0 μm is distinctly coarser than the preceding subgrain size. An even greater shear strain of 17.1 ($\varepsilon_{eq.} = 3.28$) resulted in an identical grain size of ~ 1.0 μm. Thus, the development of refined subgrains is followed by coarsening as the magnitude of the strain increases during PSM of pure Al.

Elongated, refined subgrain structures are also apparent after PSM of pure Cu involving a shear strain of 2.9 ($\varepsilon_{eq.} = 1.34$). The subgrain size is even finer after a shear strain of 3.7 ($\varepsilon_{eq.} = 1.58$), and a transition from elongated subgrains to equiaxed grain structures is apparent when the shear strain is increased to 10.8 ($\varepsilon_{eq.} = 2.75$). In contrast to the coarsening observed in the grain size data for pure Al, grain refinement appears to saturate at ~ 160–170 nm during PSM of the pure Cu for shear strains of 10.8–13.6 ($\varepsilon_{eq.} = 2.75$–3.02).

Discussion

Saturation of grain refinement

Steady-state deformation of metallic materials at elevated temperatures, i.e., $T_{DEF} \geq 0.5T_M$, has been well documented in many investigations of creep (for example [31]) as well as in studies of hot working [32]. Such steady-state behavior reflects a balance between strain hardening due to dislocation generation and storage, and softening by recovery processes which reduce the number of barriers to dislocation motion, such as forest dislocations and those in subgrain structures. The balance of hardening and recovery is usually achieved after small strains ($\varepsilon_{eq.} \ll 1.0$) at elevated temperatures due to enhanced diffusivity in the elevated temperature regime. Steady-state deformation involves plastic flow at a constant strain rate under a constant applied stress or, conversely, deformation at a constant flow stress under an imposed constant strain rate. At steady-state, the deformation microstructures often exhibit well-defined subgrains that remain equiaxed and constant in size as well as in boundary misorientation over extended intervals of strain.

Steady-state behavior has been reported [33] in SPD processing of body-centered cubic Armco Fe by HPT in the range 0.08–$0.4T_M$. The flow stress was estimated from the

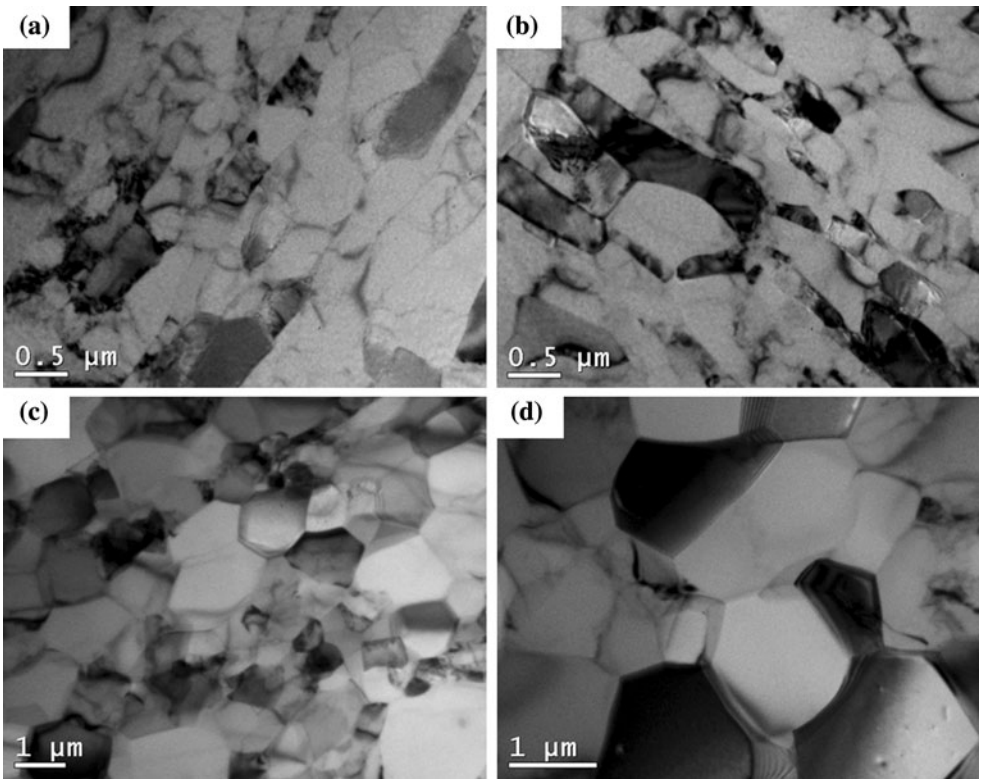

Fig. 4 TEM microstructure of PSM aluminum: **a** $\gamma = 3$, **b** $\gamma = 7$, **c** $\gamma = 11$, and **d** $\gamma = 17$

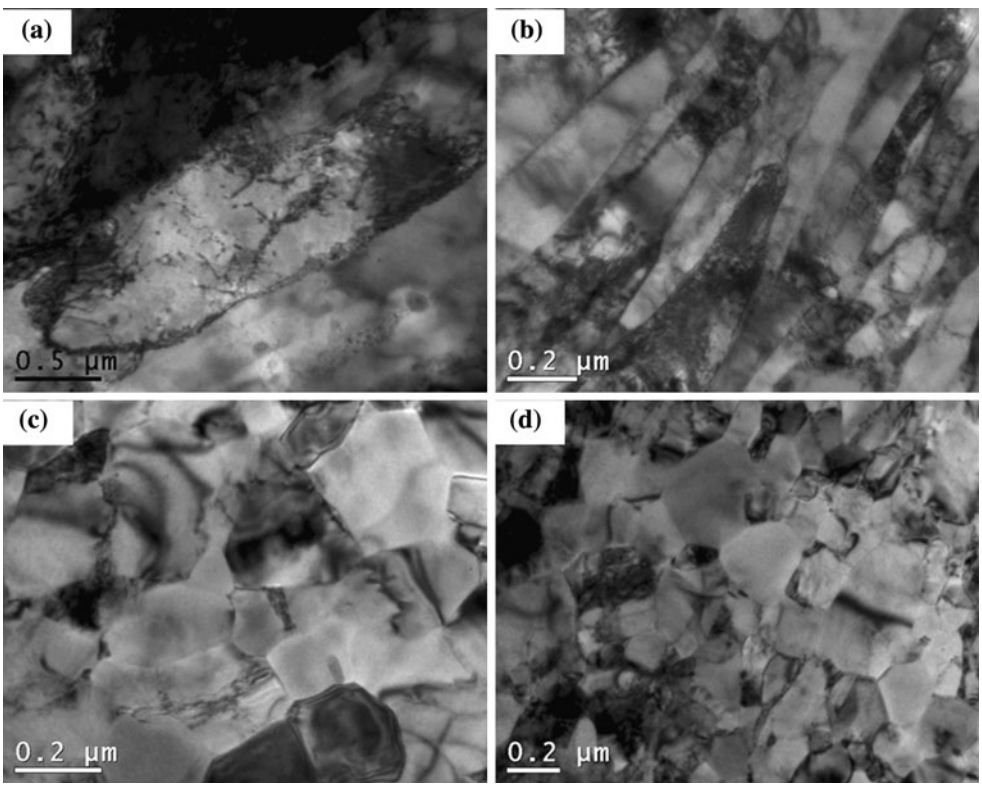

Fig. 5 TEM microstructure of PSM copper: **a** $\gamma = 3$, **b** $\gamma = 4$, **c** $\gamma = 11$, and **d** $\gamma = 14$

applied torque which depended on deformation parameters and, in this temperature regime, an increase in deformation temperature or decrease in deformation rate resulted in a decrease in the flow stress as well as the strain at onset of the steady-state. Also, the deformation-induced microstructure coarsened with these changes in deformation parameters. Saturation in grain refinement accompanied by saturation in the torque has also been reported [34] during HPT of single crystal Ni at ambient temperature ($T_{HPT} = 0.17T_M$). Saturation of grain size as well as saturation of the fractions of both high-angle and low-angle boundaries and boundary misorientations required $\varepsilon_{eq.} \approx 10$. In the current investigation, saturation in refinement of high-purity Al during repetitive ECAP was observed at a grain size of ~4.0 μm. Likewise, saturation in refinement of commercial purity Al at a grain size of ~1.0 μm was observed during HPT. In contrast, refinement followed by coarsening was observed during PSM of Al. The limited data on temperature changes during these SPD processes suggests that there are temperature increases and these increases must be considered in any analysis of grain refinement [14–16].

A model for grain size evolution

Temperature, rate of deformation, and alloy constitution are all expected to affect saturation of the flow stress and grain size. This suggests that temperature- and rate-dependent processes should be incorporated into a model for grain refinement. Furthermore, a model for refinement should also include adiabatic effects to account for temperature increases that may be appreciable during SPD. Thus, an increment in plastic work per unit volume during deformation may be expressed as

$$dW = \sigma(\varepsilon, \dot{\varepsilon}, T, s) \times \dot{\varepsilon} \times dt, \tag{6}$$

where W is the plastic work, σ is the applied stress, ε is the strain, $\dot{\varepsilon}$ is the strain rate, T is the deformation temperature, s is the mean grain size, and t is time. The plastic work done may be stored in various internal features of the sample:

$$dW = dW_v + dW_d + dW_{gb} + \cdots, \tag{7}$$

where W_v, W_d, and W_{gb} are the energies associated with vacancies, dislocations, and grain boundaries. Here, dW_{gb} will be positive when the grain size decreases, so that

$$dW_{gb} = -\gamma dS = -3\gamma \frac{ds}{s^2} = \alpha \times \sigma \times \dot{\varepsilon} \times dt, \tag{8}$$

where γ is the grain boundary energy, S is the grain boundary area, and α is the fraction of the total work done that is stored by the creation of the new grain boundary area. Equation 8 may be rewritten as:

$$\frac{ds^-}{dt} = -\alpha \times \frac{\sigma s^2}{3\gamma} \times \dot{\varepsilon} \text{ ; or, rearranging: } \frac{ds^-}{d\varepsilon} = -\alpha \times \frac{\sigma s^2}{3\gamma}, \tag{9}$$

where s^- refers to a decrease in grain size. At any temperature, there is a driving force for grain growth given by:

$$\frac{ds^+}{dt} = \frac{2\gamma}{s} \times \frac{\Omega}{\delta} \times \frac{D}{kT} \text{ ; or, again, rearranging:}$$
$$\frac{ds^+}{d\varepsilon} = \frac{2\gamma}{s} \times \frac{\Omega}{\delta} \times \frac{D}{\dot{\varepsilon} kT}, \tag{10}$$

where Ω is the volume per atom, δ is the width of the grain boundary. The diffusion coefficient, D, is given by $D = D_V + \frac{\delta}{3s} D_{GB}$, where D_V, the volume diffusion coefficient, and D_{GB}, the grain boundary diffusion coefficient, are calculated using the relationship $D = D_0 \exp\left(-\frac{Q}{kT}\right)$, with values of D_0 and Q corresponding to volume and grain boundary diffusion, respectively, and k is Boltzmann's constant. The overall kinetics of the grain size evolution as a function of strain may be obtained by combining Eqs. 9 and 10 so that:

$$\frac{ds}{d\varepsilon} = \frac{2\gamma}{s} \times \frac{\Omega}{\delta} \times \frac{D}{\dot{\varepsilon} kT} - \alpha \times \frac{\sigma s^2}{3\gamma} \tag{11}$$

If it is assumed that uniform deformation occurs under adiabatic conditions then the remainder of the work done by the applied load will be dissipated as heat and the corresponding temperature change within the sample will be given by

$$\frac{dT}{dt} = (1-\alpha) \times \frac{\sigma}{\rho C_P} \times \dot{\varepsilon} \text{ or, in terms of the strain}$$
$$\frac{dT}{d\varepsilon} = (1-\alpha) \times \frac{\sigma}{\rho C_P} \tag{12}$$

During SPD at a low homologous temperature, the flow stress dependence on grain size may be assumed to follow the Hall–Petch [35, 36] relationship:

$$\sigma = \sigma_0 + K_{H-P} \times s^{-1/2} \tag{13}$$

Together, Eqs. 11–13 constitute a system that may be solved to give the grain size as a function of strain during SPD for adiabatic conditions. The corresponding sample temperature will increase with strain according to the product of the imposed strain rate and the flow stress as it evolves during SPD.

In the event that the deformation conditions are not adiabatic, i.e., SPD occurs in the presence of a heat sink for the energy dissipated during deformation, then Eq. 12 may be modified appropriately to include this as

$$\frac{dT}{dt} = (1-\alpha) \times \frac{\sigma\dot{\varepsilon}}{\rho C_p} - \frac{\dot{Q}_{out}}{\rho C_p} \text{ ; re - arranging:}$$
$$\frac{dT}{d\varepsilon} = (1-\alpha) \times \frac{\sigma}{\rho C_p} - \frac{\dot{Q}_{out}}{\rho C_p} \times \frac{1}{\dot{\varepsilon}}, \tag{14}$$

where $\dot{Q}_{out}$ is the rate of heat sinking to the surroundings of the sample. Now, in addition to strain dependence the sample temperature increase will also depend on strain rate through the second term in Eq. 14. However, the details of heat transfer from the sample to its surroundings must also be taken into consideration to determine the effect of strain rate.

The simplest case would be to consider a planar problem where the rate of heat sinking is a linear function of the temperature increase in the sample. Under this assumption, Eq. 14 may be expressed alternatively as:

$$\frac{dT}{d\varepsilon} = (1-\alpha) \times \frac{\sigma}{\rho C_P} - \beta \times \frac{dT}{d\varepsilon} \text{ ; thus, it follows that}$$
$$\frac{dT}{d\varepsilon} = \frac{(1-\alpha)}{(1+\beta)} \times \frac{\sigma}{\rho C_P}, \quad (15)$$

where β is a coefficient describing heat transfer to the sample surroundings. Alternatively, the heat sink rate may be a linear function of the difference between the current temperature and the temperature of the sample surroundings, T_0, so that

$$\frac{dT}{d\varepsilon} = (1-\alpha) \times \frac{\sigma}{\rho C_P} - \beta(T - T_0). \quad (16)$$

Implications of the model

There are at least three different situations involving the coefficient β that may be reflected in the evolution of grain size during SPD.

1) The coefficient β is sufficiently large that $\frac{dT}{d\varepsilon} \to 0$ and deformation is isothermal. Inspection of Eq. 11 reveals that $\frac{ds}{d\varepsilon} \to 0$ only if $s \to 0$, which is not physically reasonable. Thus, under such conditions, grain refinement will be continuous. This is illustrated in the schematic plots in Fig. 6a, which show the relative refinement of the grain size as a function of strain for selected values of α in Eq. 9. The absolute rate of change of grain size with strain decreases as the assumed value of α becomes smaller, but the grain size does not saturate. The introduction of the Hall–Petch relationship, Eq. 13, will increase the absolute rate of change of the grain size with strain. Under isothermal conditions, the observation of saturations in the flow stress and grain refinement might suggest that the Hall–Petch relationship breaks down for very fine grain sizes. Indeed, an inverse grain size effect has been noted, although only at grain sizes below 10–20 nm [37–39].
2) At smaller values of β, a balance between the heat generation and heat sinking may enable sufficient grain growth to balance grain refinement and, in turn, lead to an apparent saturation in grain refinement during SPD. This can occur as temperature increases due to adiabatic heating during deformation. Accordingly, plots of relative grain size as a function of strain were determined from numerical solutions of Eqs. 11–13 for selected values of $c = \frac{2\gamma\Omega D}{\delta\varepsilon kT}$ with $\alpha = 0$ and are shown in Fig. 6b. These plots suggest that there is an incubation period before grain growth becomes apparent. This appears to reflect that some temperature rise is necessary before grains can grow, that is, the importance of the ratio $\frac{D}{\dot{\varepsilon}}$ in Eq. 11. This incubation

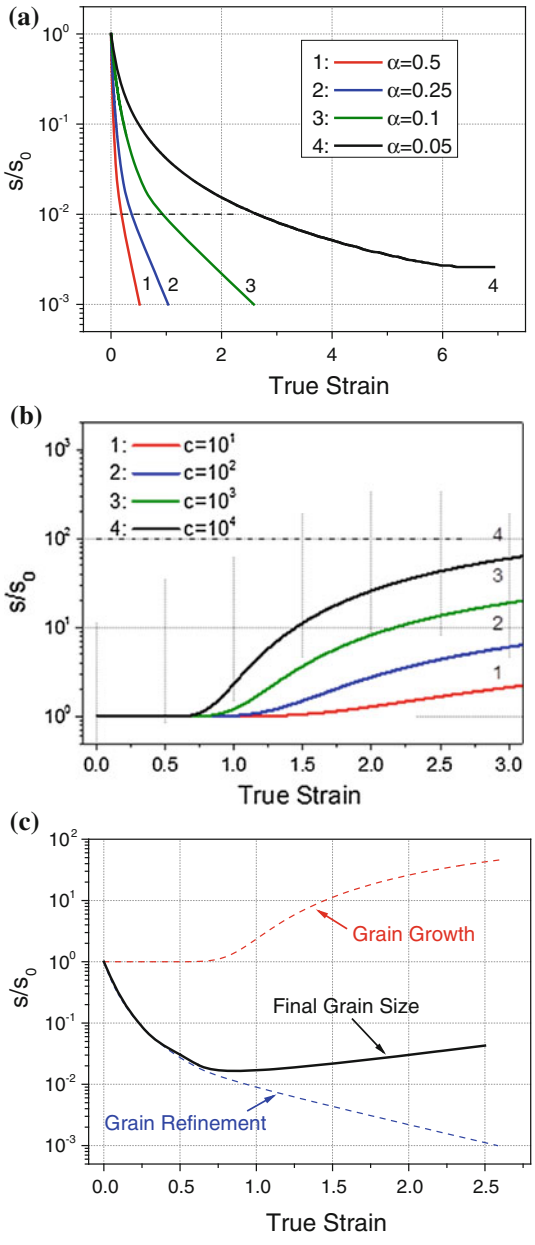

Fig. 6 Schematic of mean grain size changes in SPD processes: **a** refinement, **b** grain growth, **c** combination of refinement and grain growth

Table 1 Material parameters used in calculations

Parameters	Copper	Nickel	Aluminum
Mass density, ρ (kg/m^3)	8908	8920	2700
Heat Capacity, C_P (J/K/mol)	24.4	26.1	24.4
Atomic volume, Ω (m^3)	1.18×10^{-29}	1.09×10^{-29}	1.66×10^{-29}
Grain boundary thickness, δ (m)		1.0×10^{-9}	
Grain boundary surface energy, γ (J/m^2)		1.0	
Friction stress, σ_0 (Pa)	25.3×10^6	20.0×10^6	210×10^6
Hall–Petch coefficient, K_{H-P} (Pa/m$^{1/2}$)	77.8×10^3	111.7×10^3	99.7
Pre-exponential, D_{0V} (m^2/s)	2.0×10^{-5}	1.9×10^{-4}	1.7×10^{-4}
Volume activation energy, Q_V (J/mol)	197×10^3	284×10^3	142×10^3
Pre-exponential δD_{GB} (m^3/s)	5.0×10^{-15}	3.5×10^{-15}	5.0×10^{-14}
GB activation energy, Q_{GB} (J/mol)	104×10^3	115×10^3	84×10^3
Fraction of plastic energy for grain refinement, α	0.095		
Heat transfer coefficient, β	5×10^{-5}		

Table 2 Microstructure parameters of highly strained copper, nickel, and aluminum processed by severe plastic deformation

Copper								
Parameters	Initial	M	ECAP	ECAP +M	HPT	M + HPT	ECAP +HPT	ECAP + M+HPT
Accumulated strain	0	1.02	2.40	3.42	5.83	6.85	8.23	9.25
Mean grain size, nm (XRD)	49	10	22	9	17	13	14	13
Mean grain size, μm (TEM)	>5	–	0.5	–	0.32	0.31	0.31	0.21
Mean grain size, μm (EBSD)	–	–	–	–	0.26	0.24	0.27	0.22

Nickel								
Parameters	Initial	ECAP	ECAP +CR	HPT	HPT (10)	HPT (20)	ECAP +HPT	ECAP + CR + HPT
Accumulated strain	0	3.21	3.92	5.83	6.64	7.44	9.04	9.25
Mean grain size, nm (XRD)	–	29	25	26	26	22	24	15
Mean grain size, μm (TEM)	–	0.35	0.30	0.17	0.15	0.08	0.14	0.10
Mean grain size, μm (EBSD)	–	–	–	–	–	–	–	0.28

Aluminum								
Parameters	Initial	M	ECAP	ECAP +M	HPT	M + HPT	ECAP + HPT	ECAP + M +HPT
Accumulated strain	0	1.02	2.40	3.42	5.83	6.85	8.23	9.25
Mean grain size, nm (XRD)	0.91	0.37	0.31	0.28	0.37	0.32	0.34	0.27
Mean grain size, μm (TEM)	–	–	1.2	–	0.8	–	–	–
Mean grain size, μm (EBSD)	33.5	–	–	–	0.9	–	–	–

period is shorter for conditions leading to more rapid temperature increase with strain.

3) As $\beta \rightarrow 0$, deformation becomes adiabatic, and an initial strain interval of grain refinement may be followed by grain coarsening at larger strains. This is illustrated in Fig. 6c, wherein the combined effects of initial grain size refinement at lower SPD strains is followed by coarsening at larger SPD strains due to adiabatic heating.

Material parameters for pure Ni were obtained from the literature [40] and the grain size data acquired during HPT of pure Ni [41–44] were combined to estimate the parameters α and β (Table 1) in order to develop a numerical simulation of grain refinement during SPD. All experimental data for aluminum, copper, and nickel are summarized in Table 2. The results of this simulation are presented in Fig. 7a for Ni. Similar plots were also developed for pure Cu (Fig. 7b) and Al (Fig. 7c). In each

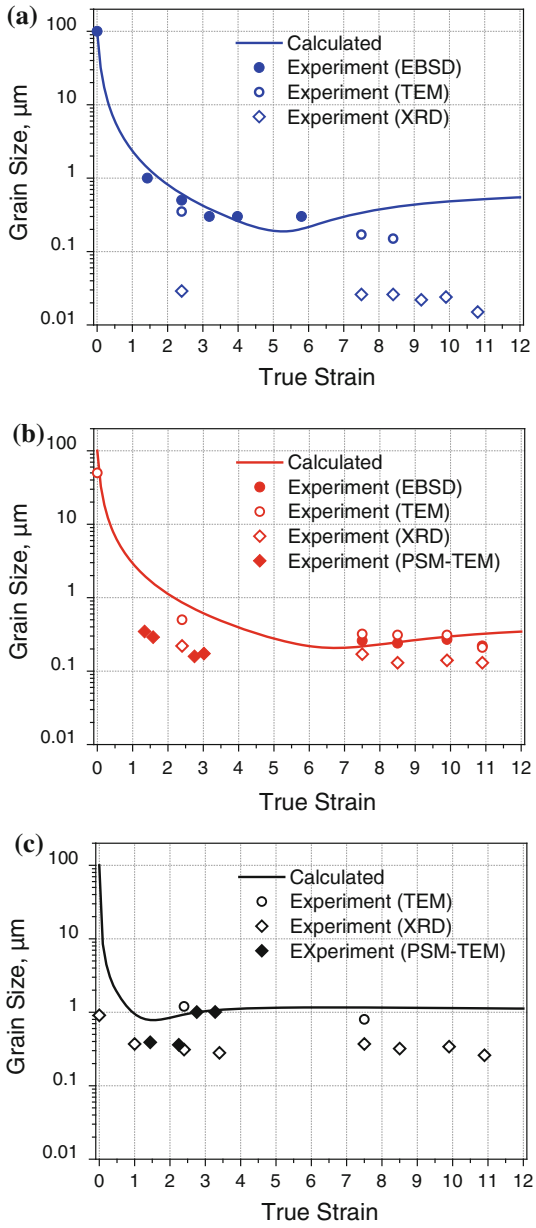

Fig. 7 Mean grain size as a function of accumulated strain for **a** nickel, **b** copper, and **c** aluminum. Experimental data are also summarized in Tables 1 and 2

case, experimental data points as well as the simulations are plotted in the form of grain size as a function of strain. The simulations of grain refinement in the Ni and Cu materials predict that the original grain size is reduced by a factor of $>10^2$ at a strain of 5–6 before gradually increasing at even larger strain values. The minimum grain sizes are about 200 nm in both the Ni and Cu simulations, and the experimental grain size data, including those obtained by PSM in the current work and summarized in Table 3, are consistent with the simulations in both cases. The finest grain size values predicted by these simulations, $\approx$200 nm, exceed those for the onset of an inverse grain size effect [37–39]. The grain size of pure Al is expected to reach a minimum at smaller SPD strains before apparently saturating at about 1.0 μm. Grain size measurements, again including those obtained in PSM in the current work, are consistent with the simulations. However, it should be noted that the crystallite size determined by XRD is actually the subgrain size, which is generally smaller than grain size values measured by OIM or/and TEM, and subgrains are not accounted in the present model. The finest subgrain sizes were measured in the Ni, which is consistent with the low initial homologous temperature during SPD of this material under ambient conditions. Further development of the model will include the influence of dislocation substructure and subgrain size.

Summary and conclusions

The following conclusions may be drawn from this investigation.

1) Many different SPD processes applied to bulk materials lead to significant refinement (by a factor of 10^2 or more) of grains to submicron or even nano-scale sizes. Often, grains appear to saturate in size or even coarsen at high SPD strains. One of the factors that may influence this saturation is adiabatic heating, which has received only limited consideration.

Table 3 Microstructure parameters of highly strained copper and aluminum processed by PSM

Material	V_0 (mm/s)	a_0 (mm)	a_w (mm)	Rake angle α (°)	Strain γ	(ε_{eq})	Grain size (nm)
Aluminum	8.3	0.11	3.84	40	3.2	1.44	390 ± 156
				30	6.9	2.25	361 ± 153
				20	10.9	2.76	1006 ± 463
				−20	17.1	3.28	1008 ± 430
Copper	18.3	0.11	3.84	40	2.9	1.34	346 ± 110
				35	3.7	1.58	290 ± 78
				−5	10.8	2.75	159 ± 69
				−10	13.6	3.02	173 ± 95

2) A model developed in this work shows that SPD under isothermal conditions should result in continuous refinement of the grain size. This reflects the hardening effect of grain refinement and a corresponding increase in flow stress as SPD straining proceeds.
3) A saturation in grain size refinement reflects a balance of refinement due to straining and grain growth due to the sample temperature rise associated with deformation under adiabatic conditions. Under adiabatic conditions, the temperature rise may lead to increases in grain size with continued SPD straining.

Acknowledgements Partial support for this work was provided by the U.S. Air Force Office of Scientific Research (Contract F1ATA06058G001, 2006-09, B. Conner, Scientific Officer). SS acknowledges support under the U.S. National Research Council Postdoctoral Fellowship Program at the Naval Postgraduate School. TGL and APZ acknowledge support by the European Research Council under ERC Grant Agreement No. 267464-SPDMETALS.

References

1. Valiev RZ, Islamgaliev RK, Alexandrov IV (2000) Prog Mater Sci 45:103
2. Segal VM, Reznikov VI, Drobyshevskiy AE, Kopylov VI (1981) Russ Metal 1:99
3. Valiev RZ, Langdon TG (2006) Prog Mater Sci 51:881
4. Iwahashi Y, Horita Z, Nemoto M, Langdon TG (1997) Acta Mater 45:4733
5. Iwahashi Y, Horita Z, Nemoto M, Langdon TG (1998) Acta Mater 46:3317
6. Zhilyaev AP, Kim BK, Szpunar JA, Baró MD, Langdon TG (2005) Mater Sci Eng A 391:377
7. Zhilyaev AP, Swisher DL, Oh-ishi K, Langdon TG, McNelley TR (2006) Mater Sci Eng A 429:137
8. Zhilyaev AP, Langdon TG (2008) Prog Mater Sci 53:893
9. Bridgman PW (1943) J Appl Phys 14:273
10. Bridgman PW (1952) Studies in large plastic flow and fracture. McGraw-Hill, New York
11. Merchant ME (1945) J Appl Phys 16:267
12. Edalati K, Horita Z (2011) Acta Mater 59:6831
13. Kim HS (2009) Mater Sci Eng A 503:130
14. Yamaguchi D, Horita Z, Nemoto M, Langdon TG (1999) Scripta Mater 41:791
15. Zhilyaev AP, García-Infanta JM, Carreño F, Langdon TG, Ruano OA (2007) Scripta Mater 57:763
16. Todaka Y, Umemoto M, Yamazaki A, Sasaki J, Tsuchiya K (2008) Mater Trans 49:7
17. Shaw MC (1984) Metal cutting principles. Oxford University Press, Clarendon
18. Iwahashi Y, Wang J, Horita Z, Nemoto M, Langdon TG (1996) Scripta Mater 35:143
19. Polakowski NH, Ripling EJ (1966) Strength and structure of engineering materials. Prentice-Hall, Englewood Cliffs
20. Onaka S (2010) Phil Mag Let 90:633
21. Brown TL, Swaminathan S, Chandrasekar S, Compton WD, King AH, Trumble KP (2002) J Mater Res 17:2484
22. Swaminathan S, Shankar WD, Lee L, Hwang J, King AH, Kezar RF, Rao BC, Brown TL, Chandrasekar S, Compton WD, Trumble KP (2005) Mater Sci Eng A 410–411:358
23. Swaminathan S, Brown TL, Chandrasekar S, McNelley TR, Compton WD (2007) Scripta Mater 56:1047
24. Terhune SD, Swisher DL, Oh-ishi K, Horita Z, Langdon TG, McNelley TR (2002) Metall Trans A 33:2173
25. Oh-ishi K, Zhilyaev AP, McNelley TR (2005) Mater Sci Eng A 410–411:183
26. Zhilyaev AP, Oh-ishi K, Langdon TG, McNelley TR (2005) Mater Sci Eng A 410–411:277
27. Zhilyaev AP, Swaminathan S, Raab GI, McNelley TR (2006) Scripta Mater 55:931
28. Zhilyaev AP, McNelley TR, Langdon TG (2007) J Mater Sci 42:1517. doi:10.1007/s10853-008-2624-z
29. Zhilyaev AP, Swaminathan S, Gimazov AA, McNelley TR, Langdon TG (2008) J Mater Sci 43:7451. doi:10.1007/s10853-012-6429-8
30. Korznikova EA, Mironov SY, Korznikov AV, Zhilyaev AP, Langdon TG (2012) Mater Sci Eng A 556:437
31. Sherby OD, Burke PM (1967) Prog Mater Sci 13:325
32. Sherby OD, Wadsworth J (1984) Deformation processing and microstructure. ASM International, Materials Park
33. Vorhauer A, Pippan R (2008) Metall Mater Trans A 39:417
34. Pippan R, Scheriau S, Taylor A, Hafok M, Hohenwarter A, Bachmaier A (2010) Annu Rev Mater Res 40:319
35. Hall EO (1951) Proc Phys Soc B 64:742
36. Petch NJ (1953) J Iron Steel Inst 174:25
37. Nieh TG, Wadsworth J (1991) Scripta Metall Mater 25:955
38. Eckert J, Holzer J, Krill C, Johnson W (1992) J Mater Res 7:1751
39. Greer JR, Dongchan J, Gu XW (2012) J Metals 64:1241
40. Frost HJ, Ashby MF (1982) Deformation-mechanism maps. Pergamon Press, Oxford
41. Zhilyaev AP, Lee S, Nurislamova GV, Valiev RZ, Langdon TG (2001) Scripta Mater 44:2753
42. Zhilyaev AP, Nurislamova GV, Kim B-K, Baró MD, Szpunar JA, Langdon TG (2003) Acta Mater 51:753
43. Zhilyaev AP, Kim B-K, Nurislamova GV, Baró MD, Szpunar JA, Langdon TG (2002) Scripta Mater 46:575
44. Zhilyaev AP, Gimazov AA, Soshnikova EP, Révész A, Langdon TG (2008) Mater Sci Eng A 489:207